

Enhancing Representation in Radiography-Reports Foundation Model: A Granular Alignment Algorithm Using Masked Contrastive Learning

Weijian Huang^{1,2,3}, Cheng Li¹, Hao Yang^{1,2,3}, Jiarun Liu^{1,2,3}, and Shanshan Wang^{1,2}

¹ Paul C. Lauterbur Research Center for Biomedical Imaging, Shenzhen Institute of Advanced Technology, Shenzhen, China

² Pengcheng Laboratory, Shenzhen, China

³ University of Chinese Academy of Sciences, Beijing, China
Sophiasswang@hotmail.com, ss.wang@siat.ac.cn

Abstract. Recently, multi-modal vision-language foundation models have gained significant attention in the medical field. While these models offer great opportunities, they still face a number of challenges, such as the requirement for fine-grained knowledge understanding in computer-aided diagnosis and capability of utilizing very limited or no task-specific labeled data in real-world clinical applications. In this study, we present MaCo, a novel multi-modal medical foundation model that explores masked contrastive learning to achieve granular alignment and zero-shot learning for a variety of medical imaging tasks. MaCo incorporates a correlation weighting mechanism to adjust the correlation between masked image patches and their corresponding reports, thereby enhancing the representation learning capabilities. We evaluate MaCo on six well-known open-source X-ray datasets, and the experimental results show it outperforms seven state-of-the-art approaches for classification, segmentation, and zero-shot phase grounding, demonstrating its great potential to promote a wide range of medical image analysis tasks.

Keywords: Multi-Modal Representation · Vision-Language Representation Learning · Medical Foundation Model

1 Introduction

Recent advances in machine learning have revolutionized the potential of automated diagnostic systems (ADS) by achieving expert-level performance, making it feasible to use deep learning to improve the clinical workflow [1, 2]. These ADS have demonstrated their efficacy in addressing various routine clinical tasks, such as disease diagnosis and lesion quantification, through training diverse machine learning models [1]. However, this traditional approach of training separate models for specific applications from scratch has inherent limitations. It is computationally expensive and demands a considerable amount of manually annotated

data, which fundamentally limits the development and scalability of medical applications [3, 4]. As a result, there is an urgent need to explore alternative approaches that can improve the effectiveness of ADS while mitigating these challenges [5].

One promising solution is to develop medical foundation models that can handle multiple clinical applications simultaneously and leverage pre-trained models to reduce the dependency on large annotated datasets [4–7]. These models can be trained on diverse and representative image-based datasets using self-supervised methods that do not require annotations, allowing them to learn robust and transferable feature representations that can be used across various tasks and domains [8]. By incorporating simple task-based heads with well-learned feature representations from the foundation model, these methods can achieve good performance in specific tasks without the need for extensive manual annotations, which are typically required in custom deep-learning training processes [9]. This reduces the labeling burden on clinical experts and enhances the potential for clinical deployment. However, as these methods are being increasingly adopted, researchers face greater challenges due to the higher precision requirements in clinical deployment environments and the need for task generalization in open environments [5, 6].

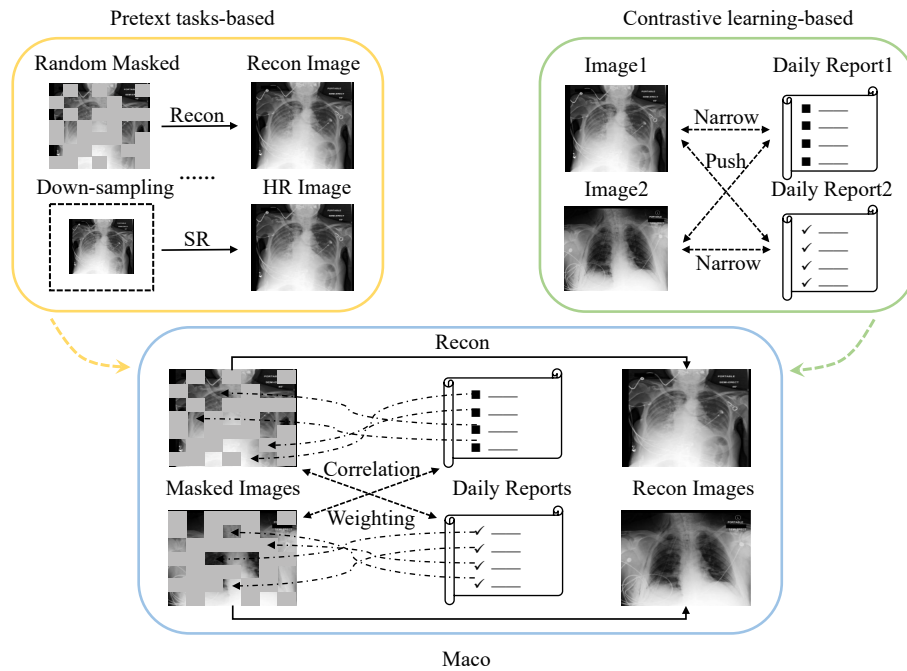


Fig. 1. The proposed MaCo framework. A novel masked contrast learning strategy is employed to leverage the advantages of both contrastive learning and pretext tasks.

Integrating expert knowledge with ADS has shown promising results, as it combines human insight with the feature distribution obtained through data-driven machine learning approaches [5, 10, 11]. This approach has the potential to generate more reliable and intuitive results, making it a valuable tool for improving the performance of ADS [3]. Coincidentally, radiology reports obtained from daily clinical examinations often contain valuable information regarding healthcare history, imaging manifestations, and disease severity. Leveraging these reports can provide a valuable source of human knowledge to augment the capabilities of ADS. However, extracting meaningful information from radiology reports remains a pressing issue due to their highly subjective and unstructured nature, which can vary depending on the individual style of the clinical physician. Effective integration rich human knowledge from radiology reports with machine learning models remains an ongoing challenging.

Researchers have been making efforts to effectively leverage expert knowledge from clinical reports [8, 12], which can be broadly categorized into two branches. One branch focuses on improving radiological representations for down-stream tasks through fine-tuning. These methods design sophisticated self-supervised pretext tasks, such as using masked autoencoders (MAE), to obtain robust image representations [9]. These representations are then integrated with the text information to enhance the performance of down-stream fine-tuning tasks [13, 14]. The other branch draws inspiration from contrastive learning approaches [15] and aims to align the feature distributions of images and texts [5, 16, 17]). These methods not only achieve comparable fine-tuning performance but also acquire zero-shot capabilities to cope with the complex and diverse clinical environment. Misra et al. [18] have suggested that finding a better balance between these methods is beneficial. However, such attempts have not yet been explored in the medical field.

In this paper, we focus on two key aspects when considering methods for building a medical vision-language foundation model. Firstly, we highlight the importance of fine-grained semantic understanding across the radiography and the clinical reports. Given the intrinsic reliance on detailed descriptions in medical knowledge [5], achieving precise semantic comprehension represents a significant step toward advancing precision medicine [10]. Secondly, we advocate for the foundation model to possess a certain level of capability even under extreme conditions of limited annotations [1], where there may be only a scarcity of labeled data for down-stream tasks. This ensures the continued effectiveness of the foundation model, even in scenarios where no annotations are available for the specific task at hand. To address these requirements, we introduce a masked contrastive medical foundation model (MaCo), which aims to achieve granular alignment to enhance feature representation. As depicted in Fig. 1, MaCo investigates the strengths of pretext task-based learning and contrastive learning while introducing a correlation weighting mechanism to enhance the capabilities of representation learning. Through extensive experiments, we have thoroughly evaluated the effectiveness of MaCo in various down-stream fine-tuning tasks, even in zero-shot learning scenarios. Experimental results demonstrate the su-

priority of MaCo over all other models. The exceptional performance achieved by MaCo in zero-shot learning tasks highlights potential to reduce annotation costs in medical applications.

2 Results

To validate the effectiveness of MaCo as a medical foundational model, we begin by evaluating MaCo’s performance on fine-tuning tasks, including segmentation and classification tasks with varying annotated sample ratios. Then, we provide qualitative and quantitative evidence to showcase MaCo’s zero-shot phase grounding capabilities. Furthermore, we also conduct a comparative analysis with non-zero-shot methods to comprehensively evaluate the effectiveness of the proposed method. Finally, visualizations of the proposed weighted mechanism are presented to demonstrate how our network accurately learns relevant regions.

2.1 Comparison of label-efficient classification

We present the fine-tuning results of various foundation models on classification tasks using the CheXpert, RSNA Pneumonia, and NIH CHEST X-RAY datasets. In particular, we evaluate the performance of MaCo when different ratios of annotated samples are provided for fine-tuning and compare it with the currently prevailing contrast learning methods.

Table 1. Comparison of AUC scores for classification performance on three open-source datasets with varying ratios of annotated samples. The term ‘Epoch’ refers to the number of epochs required for pre-training. ‘*’ denotes the MIMIC-CXR re-implemented version.

Methods	Epoch	Pretrain-dataset	RSNA			NIH			CheXpert		
			1%	10%	100%	1%	10%	100%	1%	10%	100%
ConVIRT	200	CheXpert	77.4	80.1	81.3	-	-	-	85.9	86.8	87.3
GLoRIA	50	CheXpert	86.1	88.0	88.6	-	-	-	86.6	87.8	88.1
BioViL	30+100	PubMed+MIMIC-CXR	88.1	88.4	89.1	-	-	-	-	-	-
ConVIRT*	200	MIMIC-CXR	88.8	91.5	92.7	-	-	-	87.0	88.1	88.1
GLoRIA*	50	MIMIC-CXR	89.7	91.2	92.1	-	-	-	86.5	87.5	87.8
REFERS	45	MIMIC-CXR	89.4	91.6	92.7	76.7	80.9	84.7	87.2	88.1	88.2
MedKLIP	60	MIMIC-CXR	87.3	88.0	89.3	77.2	78.9	83.2	-	-	-
M-FLAG	100	MIMIC-CXR	-	-	-	62.2	71.6	78.7	-	-	-
MaCo	30	MIMIC-CXR	91.2	92.2	93.3	79.4	83.6	85.5	88.0	88.2	88.2

To begin with, we compare the results of models pretrained on two different datasets, CheXpert and MIMIC-CXR (Table 1). It can be observed that models trained on the MIMIC-CXR dataset (ConVIRT* and GLoRIA* in Table 1) achieves better results than those trained on the CheXpert dataset (ConVIRT and GLoRIA in Table 1). This performance discrepancy can be attributed to

the larger dataset size of MIMIC-CXR (377,110 images) compared to CheXpert (191,229 images), which is particularly beneficial for contrastive learning methods [15]. Notably, MaCo consistently outperforms other contrastive learning-based methods across various datasets and annotated sample ratios. One key advantage of MaCo over the compared methods lies in its incorporation of a pretext task in the image branch, which enables MaCo to learn improved image features and achieve enhanced performance in down-stream tasks. Additionally, Table 1 also provides information about the number of epochs required for pre-training for each method. This metric serves as an indicator of the method’s effectiveness in learning robust features, especially when dealing with large-scale datasets where an excessive number of epochs might be impractical. Remarkably, MaCo demonstrates surprising efficiency by completing the training process in just 30 epochs, significantly reducing the training time compared to alternative methods. The efficient learning capability of MaCo makes it particularly suitable for scenarios where computational resources are expensive to obtain.

Table 2. Disease-level classification performance on the NIH CHESTX-RAY dataset. The AUC scores are reported under varying ratios of training annotations.

Labeling Ratios	Methods	Average	Atelectasis	Cardiomegaly	Consolidation	Edema	Effusion	Emphysema	Fibrosis	Hernia	Infiltration	Mass	Nodule	Pleural Thickening	Pneumonia	Pneumothorax
		1%	MedKLIP	77.2	-	-	-	-	-	-	-	-	-	-	-	-
	M-FLAG	62.2	-	-	-	-	-	-	-	-	-	-	-	-	-	-
	REFERS	76.7	77.5	85.6	78.6	84.9	85.4	79.5	72.3	77.1	67.5	76.2	66.5	71.6	69.3	81.7
	Model Genesis	70.3	72.1	67.1	75.8	76.1	80.6	72.6	64.8	73.5	65.7	65.2	62.2	67.6	64.8	76.2
	C2L	71.1	75.1	67.1	77.6	75.1	83.4	71.5	66.8	70.0	63.8	70.1	66.2	68.1	65.7	74.4
	Context Restoration	67.8	69.1	64.4	73.2	73.8	78.1	70.0	62.1	70.2	65.2	62.4	59.1	65.0	62.2	73.8
	TransVW	71.3	74.5	68.9	76.7	79.8	81.1	67.9	68.7	68.2	66.8	66.5	66.2	68.5	68.8	75.0
	ImageNet Pre-training	69.8	73.3	69.6	76.0	81.7	80.5	67.1	64.9	64.8	65.8	67.0	62.3	65.7	65.0	74.0
	MaCo	79.4	77.0	91.1	79.3	87.5	87.4	88.2	71.9	85.9	67.8	88.2	96.7	80.3	70.1	84.6
10%	MedKLIP	78.9	-	-	-	-	-	-	-	-	-	-	-	-	-	-
	M-FLAG	71.6	-	-	-	-	-	-	-	-	-	-	-	-	-	-
	REFERS	80.9	80.1	89.8	79.5	87.8	87.5	88.2	77.2	86.1	69.6	82.0	72.8	74.2	72.2	85.6
	Model Genesis	76.0	77.2	72.8	77.5	85.7	85.2	81.0	75.3	78.0	68.4	73.1	69.5	72.2	67.7	80.4
	C3L	76.6	78.0	75.5	77.5	84.1	85.7	81.2	73.7	79.5	67.4	77.5	71.7	72.0	67.3	81.9
	Context Restoration	73.8	75.5	70.6	77.1	84.5	84.2	79.4	73.1	67.5	68.1	70.9	66.9	71.7	65.2	79.1
	TransVW	74.4	76.5	70.8	77.6	83.0	84.8	79.7	69.9	74.7	68.5	72.1	68.3	72.4	63.2	79.6
	ImageNet Pre-training	74.4	74.2	79.8	75.9	85.7	83.2	80.4	72.1	74.0	64.1	71.7	65.6	69.6	66.2	79.7
	MaCo	83.6	81.9	91.5	80.8	89.3	88.5	92.0	83.5	92.2	70.4	85.9	97.4	177.4	177.4	287.1
100%	MedKLIP	83.2	-	-	-	-	-	-	-	-	-	-	-	-	-	-
	M-FLAG	78.7	-	-	-	-	-	-	-	-	-	-	-	-	-	-
	REFERS	84.7	83.0	92.3	82.1	90.2	88.7	91.4	83.9	93.3	74.1	85.5	76.7	78.5	77.0	89.1
	Model Genesis	81.0	78.8	84.5	79.2	87.8	86.6	89.7	81.0	85.2	71.1	81.9	73.2	75.8	73.0	85.6
	C4L	82.2	81.1	90.2	81.0	88.1	88.0	88.3	80.8	86.8	72.0	82.7	74.1	76.2	75.3	85.9
	Context Restoration	78.7	75.8	82.9	76.4	86.6	84.8	88.2	78.6	83.0	70.0	79.6	69.5	73.2	69.4	84.0
	TransVW	81.7	79.8	85.0	80.0	88.2	87.1	90.1	81.8	85.9	72.3	82.6	74.4	76.6	74.0	86.1
	ImageNet Pre-training	80.0	78.3	89.3	77.6	87.9	85.9	87.4	78.5	88.8	65.9	79.9	70.7	74.5	71.0	84.7
	MaCo	85.5	83.8	92.9	82.3	90.7	89.3	98.5	89.3	93.5	72.0	87.2	277.5	580.0	78.1	189.3

In Table 2, the results of different methods on disease-level classification with the NIH ChestX-ray dataset are listed. Here, we introduce some additional image-based pretext task methods (i.e., Model Genesis [19], C2L [20], Context Restoration [21], TransVW [22] and ImageNet Pre-training [23]) to validate our method in a wider range. Since MedKLIP did not provide detailed category-level results, only the average AUC is reported. By exploiting the rich information provided in medical reports, MedKLIP obtains higher performance than those methods that rely solely on images. This again confirms the effectiveness of incorporating medical reports in pre-training models. Nevertheless, our MaCo can still outperform MedKLIP with AUC scores of 79.4% vs 77.2%, 83.6% vs 78.9%, and 85.5% vs 83.2% at annotated sample ratios of 1%, 10% and 100%, respectively.

Overall, MaCo outperforms currently state-of-the-art algorithms and achieves the highest classification performance on all the three investigated open-source classification datasets at different annotated sample ratios. In the meantime, MaCo’s training is more efficient, requiring much less training time compared to alternative methods. Both aspects validate the effectiveness of MaCo for fine-tuning classification tasks, making it a highly promising method for clinical applications.

2.2 Results of label-efficient segmentation

In this section, we discuss the segmentation results obtained by different methods through fine-tuning with 1%, 10% and 100% annotated data. We conducted experiments on the SIIM dataset, and compared our MaCo with four state-of-the-art methods, including ConVIRT, GLoRIA, MGCA, M-FLAG and Med-UniC. Results are provided in Table 3.

Table 3. Comparison of Dice scores for segmentation performance on SIIM with varying ratios of annotations.

Methods	1%	10%	100%
ConVIRT	25.0	43.2	59.9
GLoRIA	35.8	46.9	63.4
MGCA	49.7	59.3	64.2
M-FLAG	52.5	61.2	64.8
Med-UniC	56.7	62.2	64.4
MaCo	58.8	70.7	89.6

Our MaCo consistently outperforms the other approaches in all experiments. Specifically, at a small annotated sample ratio of 1%, MaCo achieves slightly better performance than the current state-of-the-art method, Med-UniC. As the annotated sample ratio increases, MaCo demonstrates significant improvement in performance. At the annotated sample ratio of 10%, MaCo achieves a notable boost in performance with a Dice score of 70.7%, surpassing Med-UniC, which

achieves a Dice score of 62.2%. This highlights MaCo’s ability to capitalize on additional labeled data to enhance its feature representation and segmentation accuracy.

These experiments highlight the advantages of MaCo in terms of segmentation performance with increasing levels of annotation, showcasing its potential in reducing the reliance on manual labeling and improving the efficiency of medical data analysis.

2.3 Results of zero-shot phase grounding

Interpretable visualization of the correlations between modalities is necessary to establish clinical trust and remove barriers to clinical application. Phase grounding serves as an effective tool to achieve this purpose. Here, we evaluate the zero-shot phase grounding performance of MaCo on the MS-CXR dataset, which provides medical freely sentences and corresponding bounding boxes.

Notably, thanks to the proposed variable alignment module, we were able to utilize the weight map shown in Fig. 4. We first applied the softmax function along the pixel dimension (denoting the related patch weight) of the final weight map, with a soft threshold τ . We then multiplied the resulting weights with the patch-based similarity matrices computed from the image modalities. Finally, the latent features of images and reports were calculated to obtain mean Intersection over Union (mIoU) and contrast-to-noise ratio (CNR).

Table 4. Comparison of zero-shot phase grounding for segmentation performance on MS-CXR datasets.

Methods	mIoU	CNR
ConVIRT	0.238	0.818
GLoRIA	0.246	0.930
BioViL	0.266	1.027
MaCo	0.267	1.176

In Table 4, we compare the phase grounding performance of MaCo with three existing methods, including ConVIRT, GLoRIA, and BioViL. As the first method in the medical field to achieve zero-shot capability using discriminative approaches, ConVIRT achieves a mIoU of 0.238 and a CNR score of 0.818. Among the three comparison methods, BioViL obtains the highest metrics with a mIoU of 0.266 and a CNR of 1.027, which is likely to be benefitted from the word-weighting approach proposed in GLoRIA and using a larger pretraining dataset. Our proposed MaCo, on the other hand, achieves better scores than all three comparison methods with a mIoU of 0.267 and a CNR of 1.176. The superior performance of MaCo can be attributed to the fine-grained alignment achieved by the interaction of mask autoencoder and contrastive learning.

Qualitative phase grounding results are presented in Fig. 2, where each row represents an instance’s visual-textual correlation heatmap obtained from dif-

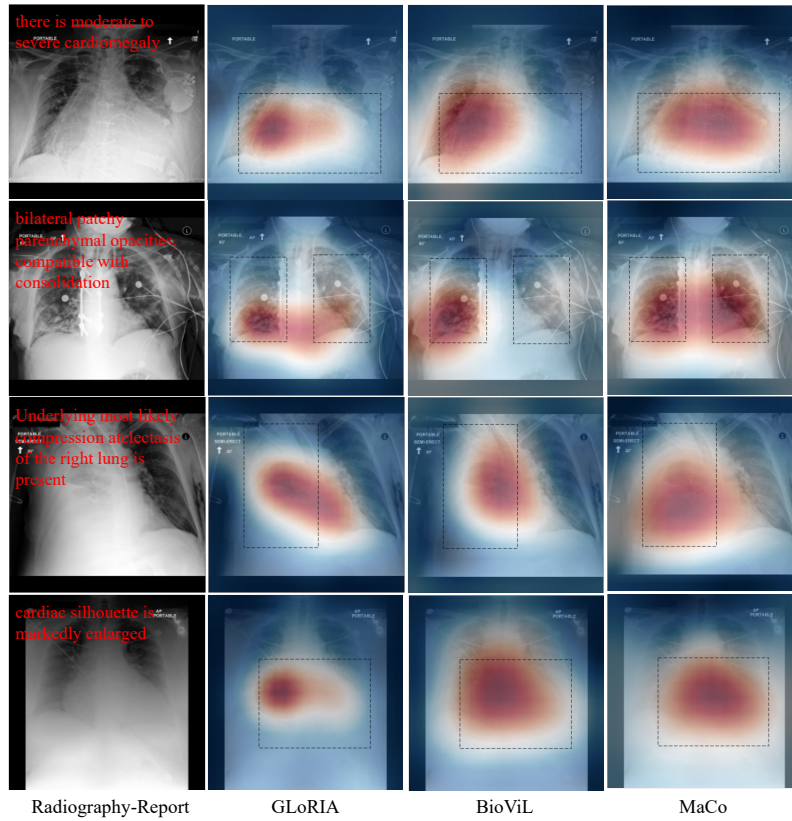


Fig. 2. Phase grounding with free-text. We visualize the association of vision and language on the MS-CXR dataset. In the first column, the free-text annotations are marked in red font, while the gold standard annotations outlined by clinical experts are represented with dashed boxes.

ferent methods. We showcase examples of diseases from different anatomical regions, including cardiomegaly, opacity, and atelectasis. In the first example, GLoRIA and BioViL only partially capture the disease, while MaCo focuses on a more complete disease region. In the second example, we provide a patient case with multiple lesions. Here, BioViL extracts information from only one of the lesions, whereas MaCo and GLoRIA can find both regions, with MaCo displaying a more comprehensive representation. Similar conclusions can be drawn from the fourth and fifth examples that MaCo exhibits better textual-visual correlations compared to GLoRIA and BioViL.

The above results demonstrate the effectiveness of MaCo in zero-shot phase grounding. In the quantitative evaluation, we compared MaCo with three popular methods and MaCo achieved better results. In the qualitative analysis, we showcased MaCo’s superior performance in establishing textual-visual correla-

tions. These results collectively emphasize the potential of MaCo as a powerful tool for interpreting multi-modal medical data.

2.4 Comparison to methods without zero-shot capability

Zero-shot capability is a crucial and highly desirable skill in clinical applications. It enables task generalization and allows for the demonstration of learned visual-language associations in phase grounding, thereby fostering trust among clinical practitioners. Nevertheless, we conduct comparative analyses between MaCo and several methods lacking zero-shot capability to obtain a more comprehensive evaluation.

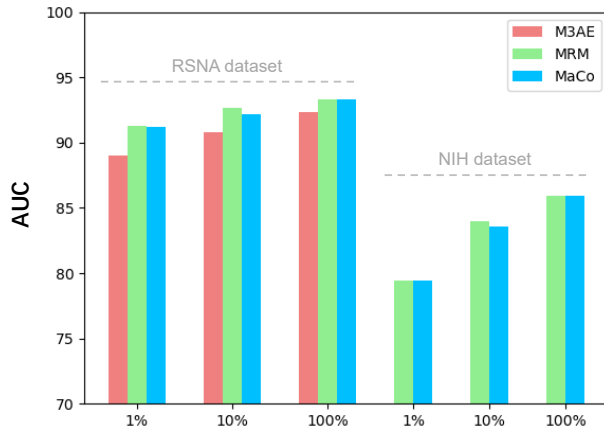


Fig. 3. Comparison of classification performance with state-of-the-art non-contrastive learning methods, taking into consideration their trade-off in sacrificing the capability of zero-shot learning.

We conduct comparative analyses between MaCo and two state-of-the-art methods lacking zero-shot capability, M3AE and MRM. Classification experiments were performed on two datasets, RSNA and NIH, and the results are shown in Fig. 3. MRM adopts both masked recovery and super-resolution as the pretext tasks, achieving the highest performance and appearing to surpass current contrastive learning-based methods. However, it should be noted that both MRM and M3AE sacrifice the zero-shot capability, as well as text-image explainability and visualization, in order to achieve their high performance. This trade-off may potentially reduce their scalability and practicality in real-world clinical applications. In contrast, MaCo achieves classification performance comparable to MRM while retaining the advantages of zero-shot capability and text-image correlation visualization. Moreover, the slight performance gap between MaCo and MRM may be compensated for in the future by exploiting the continuously

accumulated daily clinical examination data, as larger datasets have been shown to have a more significant impact on contrastive learning-based methods [15, 18].

2.5 Visualization of Granular Alignment Mechanism

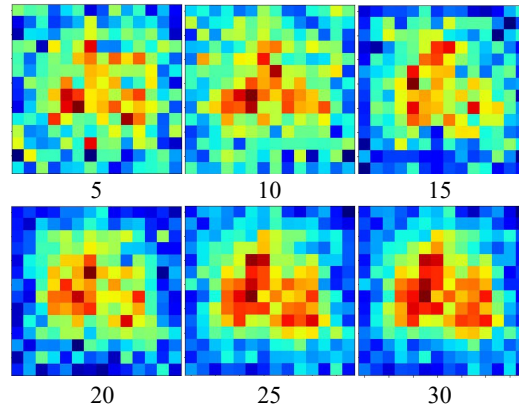


Fig. 4. Visualization of the linear weights of the proposed correlation weighting. The number under the picture indicates the training epoch. After training, the linear weights are larger in regions with a higher incidence of disease and smaller in the background regions around the edges.

To verify the effectiveness of the proposed correlation weighting, we visualize the linear weights proposed in Section 3.3.3, as shown in Fig. 4. Each pixel in the visualization corresponds to the weight assigned to an image patch. During the initial training stage, the weights are dispersed without prominent positions, indicating that the network has yet to learn the distinctions between different patches. As the training progresses over epochs, the weights in the central region of the image (typically representing the lungs) gradually increase, while the weights in the background regions decrease. This shift indicates that the model assigns greater importance to image patches near the lungs, considering them to contain more informative content compared to the background regions. The weight map not only visualizes the model’s attention on different patch positions but also holds the potential to enhance down-stream task performance, as demonstrated in the following analysis.

In Fig. 5, we illustrate the variation in mIoU and CNR scores with different τ values when multiply to the logits during testing, as mentioned in section 2.3. Since the comparison methods do not have this interaction mechanism, their indicators will not change with τ . The best-performing τ value for MaCo was determined to be 0.1, resulting in a mIoU score of 0.267 and a CNR score of 1.176. In comparison, BioViL achieves a mIoU score of 0.266 and a CNR score of 0.1027.

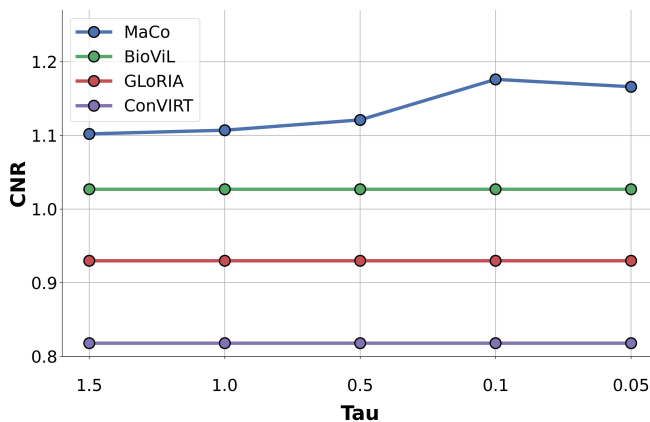


Fig. 5. Zero-shot phase-grounding performance on MS-CXR dataset. We plotted score curves for different τ (Tau) values. The peak values of MaCo’s CNR were achieved at $\tau = 0.1$.

2.6 Effectiveness of granular alignment and weighting mechanism

In this section, we compare our proposed method to the baseline approaches to highlight the effectiveness through classification and phase grounding, as shown in Table 5.

Table 5. Comparison of phase grounding and classification performance between the proposed MaCo and baseline methods.

Methods	MS-CXR			RSNA		
	mIoU	CNR	PG	1%	10%	100%
MAE	-	-	-	81.3	82.1	91.2
+CLIP	0.211	0.928	0.366	90.9	92.1	93.0
+Interaction Weighted	0.267	1.176	0.429	91.2	92.2	93.3

We treat the MAE trained solely on the image modality as our baseline model. Since MAE lacks the ability to interact with reports, its grounding capability is limited. MAE achieves an AUC of 81.3% on the RSNA dataset with 1% annotated samples. We then introduced CLIP into MAE (denote as +CLIP) to achieve granular alignment. By leveraging contrastive learning, MAE+CLIP gains zero-shot capabilities and achieves a mIoU of 0.211 in the grounding task on the MS-CXR dataset. Additionally, we observe improvement in the classification task as well, indicating that the inclusion of expert knowledge from medical reports can enhance the model’s classification performance.

Finally, we added the proposed correlation weighting mechanism. Better results are obtained, particularly in phase grounding, where there is a significant improvement in mIoU (0.267 vs. 0.211). This suggests that the model’s feature

representation capabilities were enhanced by incorporating the relevance weighting mechanism.

3 Methods

The high cost of annotation has long been a persistent challenge in the medical field. One prevalent approach to alleviate the annotation requirements in down-stream tasks is the utilization of pre-trained models. With the rapid advancements in natural language processing models in recent years, there has been a growing interest in integrating expert knowledge from clinical reports with medical images. In the following sections, relevant studies in the medical domain, specifically within the realm of self-supervised pretext task-based and contrastive learning models, will be introduced. These studies serve as the foundation for our proposed MaCo.

3.1 Pretext tasks-based methods

The goal of pretext task-based methods is to learn image representations that are semantically meaningful without utilizing any downstream task annotations [24,25]. These pretext tasks typically involve self-supervised learning techniques, such as using randomly augmented images or training on down-sampled images for super-resolution purposes. One widely utilized pretext task-based method is MAE. MAE [9] applies a random masking technique to image patches within the input data. Subsequently, a reconstruction decoder is employed to recover the masked regions. By engaging in the reconstruction process, MAE is able to learn image features that can be subsequently utilized for down-stream tasks. Due to its simplicity and effectiveness, MAE has gained considerable popularity, including in the domain of medical image-text modeling. Drawing inspiration from MAE, Zhou et al. [13] employed a similar masking mechanism in both the text branch and the image branch of their model (MRM). They leveraged the vision representation as a supplementary component to the text branch and enhanced the feature representations through back-propagation optimization. Similar to MRM, Chen et al. [14] also employed masking in both the image and text encoders in their method with a more intricate approach to integrate and couple the features of the image and text modalities (M3AE).

Although the aforementioned methods have shown promising performance in down-stream fine-tuning tasks, their zero-shot capability is constrained by the modality coupling approach. This limitation can impede their ability to generalize to new tasks, especially when dealing with unlabeled datasets.

3.2 Contrastive-learning-based methods

Contrastive learning-based methods, on the other hand, has recently gained significant attention from researchers due to its unique zero-shot capability [26,27]. Contrastive learning aims to minimize the similarity distance between paired

data points within a training batch while simultaneously maximizing the dissimilarity from other unpaired feature representations. By leveraging this approach, the trained model becomes proficient in differentiating between paired and unpaired images and texts, thereby acquiring the ability to generalize to unseen data samples, known as zero-shot capability [28].

Zhang et al. [28] were pioneers in introducing contrastive learning as a proxy task in the field of medicine. Their study demonstrated the efficacy of contrastive learning within the medical domain. Building upon this foundation, Wang et al. [29] further investigated the impact of false negative samples on the performance of contrastive learning methods. Boecking et al. [17] recognized the distinct language patterns found in medical reports, prompting a redesign of the language model for medical vision-language processing. Bannur et al. [30] and Zhou et al. [8] employed past radiology images and multi-view images, respectively, for joint training purposes. In more recent developments, Wu et al. [5] and Zhang et al. [10] integrated a report filter to extract medical entities and employed a more complex modal fusion module to aggregate features, thereby achieving improved results. On the other hand, to establish fine-grain representation between images and reports, Huang et al. [16] proposed a local fine-grained weighting mechanism. This mechanism calculates the similarity between each word and image patches, resulting in word-level responses. Similarly, Wang et al. [31] introduced the concept of multi-granularity alignment to explicitly learn the correspondence between fine-grained vision and text tokens.

These contrastive learning-based methods have achieved comparable performance in down-stream finetuning tasks to those pretext task-based methods. More importantly, some methods, such as BioViL and GLoRIA, have demonstrated inspiring zero-shot capabilities, which greatly enhance the task generalization capability of medical models.

3.3 MaCo

We introduce MaCo, a masked contrastive learning medical radiography-reports foundation model with zero-shot capability for down-stream tasks. The motivation behind MaCo is to leverage the advantages of both contrastive learning-based and pretext task-based methods to acquire enhanced semantic latent representations. We employ a masked autoencoder along with contrastive learning to facilitate learning on paired radiological images and medical reports. Additionally, we propose a correlation weighting mechanism that weights the contrastive loss based on the importance of sampled image patches. Fig. 1 shows the framework of MaCo, which joins the strengths of contrastive learning and pretext task methods. Fig. 6 illustrates the weighting mechanism. The detailed methodology will be introduced in the subsequent sections.

Radiography Mask-Auto-Encoding To extract meaningful feature representations from input images, MaCo incorporates a vision encoder that maps the observed signal to a latent representation. In this work, we adopt MAE proposed by He et al. [9] as our primary image representation extractor.

The input image is divided into regular, non-overlapping patches, and a subset of patches is randomly sampled while removing the remaining ones. This subset of patches is selected as the input, and the image encoder employed in MaCo uses a vision transformer to generate the feature representations for each patch. The vision transformer applies self-attention mechanisms to the input patches, enabling the modeling of complex spatial relationships and the capturing of long-range dependencies. The output of the image encoder is a set of feature representations, one for each input patch.

Let $v_{recon} \in \mathbb{R}^{B \times N \times C}$ denotes the batch of embeddings for the masked reconstruction patches, and $g_{recon} \in \mathbb{R}^{B \times N \times C}$ denotes the corresponding embeddings for the ground truth patches. Here, B , N , and C represent the batch size, the number of sampled patches, and the dimension of the embeddings, respectively. We use a simple Mean-Square-Error as the reconstruction loss function:

$$\mathcal{L}_{mae} = (v_{recon} - g_{recon})^2 \quad (1)$$

Report Embedding We adopt Bert [32], a classical natural language processing model that has achieved outstanding performance across various language understanding tasks, to extract expert knowledge from clinical daily examination reports.

The clinical reports are processed by dividing them into multiple sentences. In this preprocessing step, we also incorporate random sentence selection and shuffling. Next, we use a wordpiece tokenizer to convert the preprocessed reports into a sequence of numerical tokens that can be processed by Bert. The wordpiece tokenizer breaks down each word into subword units and maps them to their corresponding numerical representations. This allows Bert to capture the meaning of the text at a more granular level, improving the quality of the sentence representations. Finally, we feed the sequence of numerical tokens into Bert to obtain sentence representations. These sentence representations capture the main ideas and themes from the clinical reports and will be used to interact with the extracted image representations, which will be discussed in the next section.

Granular Alignment Mechanism In the previous two sections, we have introduced the masked image encoder and report encoder. Now, we focus on aligning the image and text in the feature space to enable zero-shot capabilities. Two challenges must be addressed in this feature alignment step: 1) Do the randomly masked images still retain sufficient information that can be correlated with the corresponding reports? 2) If yes, what is the extent of the correlation? Answering these two questions is crucial for establishing meaningful correlations between the image and the text modalities. From the perspective of a clinical expert, the answer to these two questions depends on the quality of the sampled patches. If the sampled patches can precisely cover the entire lesion area, the two modalities should be highly correlated. Otherwise, the correlation will be low.

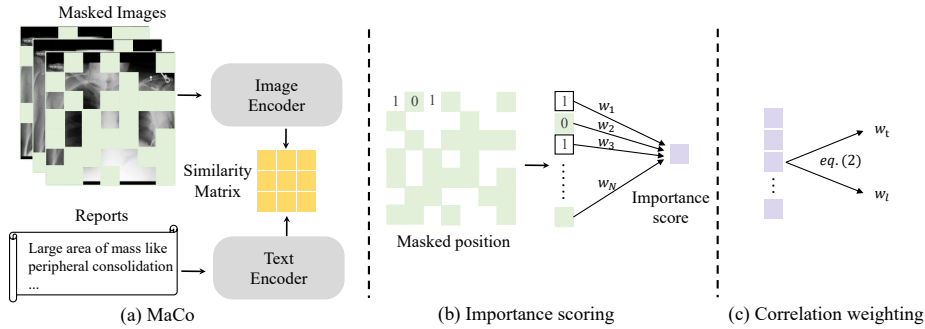


Fig. 6. The proposed correlation weighting mechanism. (a) Overview of MaCo. We encode masked radiology images and compare them to medical reports using a contrastive loss. (b) The method to generate the importance score. (c) The method to build the correlations. Two weighting coefficients are derived, with w_t to adjust the temperature coefficient for the similarity matrix and w_l to weight the contrastive loss.

We propose a correlation weighting mechanism to model the experts’ practice. The details are depicted in Fig. 6(b and c). Specifically, we score the sampled images based on the relevance masked position map. These scores are then used to adjust the temperature in contrastive learning and the weights in the loss function. By doing so, highly correlated paired samples are given a higher weight during the network learning process.

We first create a binary image according to the mask used for radiography mask-auto-encoding, assigning a value of 0 to the masked regions and a value of 1 to the unmasked regions. Next, an importance score of the image is learned by summarizing the mask information with learnable parameters, resulting in a global representation of the masked regions, as shown in Fig. 6(b).

Subsequently, two weighting coefficients are derived from the importance scores, $w_t \in \mathbb{R}$ and $w_l \in \mathbb{R}$, where w_t serves as the temperature coefficient for the similarity matrix, and w_l is utilized to weight the loss term, as shown in Eq.2.

$$w_t = \exp\left(\frac{\exp(p/\tau_1)}{\sum_d^D \exp(p_d/\tau_1)}\right),$$

$$w_l = \frac{\exp(p/\tau_2)}{\sum_d^D \exp(p_d/\tau_2)}$$
(2)

where $p \in \mathbb{R}^{B \times 1}$ represents the batch of importance scores obtained from a fully connected layer for a set of sampled instances. Please note that, as the weight coefficient of the loss function, w_l does not contribute to the gradient during training. $D \leq B$ is a mini-batch used to prevent gradient vanishing when B is large.

Then, we use w_t to adjust the temperature coefficient of the similarity matrix in Fig. 6(a). We employ w_l as the weight for the contrastive loss function.

Consequently, our contrastive loss can be expressed as:

$$\mathcal{L}_{align} = -w_l \cdot \log\left(\frac{\exp(\langle v, t \rangle / (w_t \cdot \tau_3))}{\sum_k^B \exp(\langle v, t_k \rangle / (w_t \cdot \tau_3))}\right) \quad (3)$$

where $\langle v, t \rangle$ represents the cosine similarity between the masked visual representation $v \in \mathbb{R}^{B \times C}$ and report representation $t \in \mathbb{R}^{B \times C}$. τ_1 and τ_2 are two fixed hyperparameters. τ_3 is a learnable parameter, similar to [15].

The final loss function to train our MaCo framework is:

$$\mathcal{L} = \lambda \mathcal{L}_{mae} + (1 - \lambda) \mathcal{L}_{align} \quad (4)$$

Here, λ is a hyperparameter to balance the contributions of the two loss terms.

3.4 Datasets

We pretrain MaCo using radiograph and clinical reports from the MIMIC-CXR V2 dataset [33]. To assess the transferability of the learned radiograph representations, we perform end-to-end fine-tuning on X-ray based classification and segmentation tasks. Specifically, we evaluate the pre-trained model on three X-ray datasets for classification tasks, including NIH ChestX-ray [23], CheXpert [34], and RSNA Pneumonia [35]. For the segmentation task, we fine-tune the pre-trained model using the SIIM-ACR Pneumothorax [36] dataset. Finally, for the zero-shot phase-grounding, we employ the MS-CXR dataset [17].

MIMIC-CXR v2 is a large dataset comprising 377,110 chest x-rays associated with 227,827 clinical reports sourced from the Beth Israel Deaconess Medical Center between 2011 and 2016. During pretraining, we used all paired data, regardless of whether it was frontal or lateral.

CheXpert releases a multi-label dataset for chest X-ray classification. To evaluate the performance of our model, we followed the official guidelines outlined in [34] and reported results for five selected pathologies. As the official CheXpert test set is not publicly available, we adopted a similar approach as described in [28] and used the official validation set as our test set. Additionally, following [13], we sampled 5,000 images from the official training set to construct our validation set. The resulting training/validation/test split consists of 218,414/5,000/234 images, respectively, representing the entire dataset.

RSNA Pneumonia (RSNA) introduces a binary classification problem, where each chest radiograph is classified as either pneumonia or normal. We adhere to the official data split, which consists of a training set of 25,184 images, a validation set of 1,500 images, and a test set of 3,000 images.

NIH ChestX-ray (NIH) contains 112,120 frontal-view chest radiograph images and focuses on a multi-label classification problem involving 14 different chest pathologies. The dataset is split into training, validation, and test sets, with each set comprising 70%, 10%, and 20% of the total dataset, respectively.

SIIM-ACR Pneumothorax Segmentation (SIIM) is curated to facilitate the development of segmentation models for identifying pneumothorax disease

in chest radiographs. The dataset includes more than 120,000 frontal-view chest X-rays, each accompanied by precise manual segmentation of pneumothorax regions. To construct the training, validation, and test sets, we followed the same practice as described in [16], where each set comprising 70%, 15%, and 15% of the total dataset, respectively.

MS-CXR provides annotations in the form of bounding boxes and sentence pairs that describe clinical findings observed in chest X-ray images. Each sentence describes a single pathology present in the image, and there could be multiple manually annotated bounding boxes associated with the description of a single radiological finding. The annotations were collected on a subset of MIMIC-CXR images, which contains labels across eight different pathologies. In total, 1,162 annotations of 881 cases were collected, and we utilized the entire dataset to measure the overlap between labeled bounding boxes and the results of vision-language association after pretraining.

3.5 Implementation details

For the sake of convenience and comparability, we utilized the widely-used image encoder ViT-B/16 and employed Bert with a width of 768 as our text encoder. We set the training batch size to 512 and employed the AdamW optimizer, with an initial learning rate of $4.5e-4$, weight decay of 0.05, β_1 of 0.9, and β_2 of 0.95. We set the value of λ in Eq. 4 to 0.9, and mini-batch D in Eq. 2 to 16. We set τ_1 and τ_2 in Eq. 2 to 1 and 16, respectively, while initialized the learnable parameter τ_3 in Eq. 3 to 0.03 according to the experiments.

For finetuning on the segmentation dataset SIIM, we trained the segmentation network using the AdamW optimizer, with an initial learning rate of $5e-6$, weight decay of 0.05, β_1 of 0.9, and β_2 of 0.999. For finetuning on classification datasets including CheXpert, RSNA Pneumonia, and NIH ChestX-ray, we used the SGD optimizer with a momentum of 0.9. We searched for the optimal learning rate from $8e-3$ to $1e-4$ to maximize the performance on the validation set. In both the pre-training and fine-tuning stages of the image classification task, we warmed up the network by linearly increasing the learning rate to the set value, and then decreased the learning rate according to the cosine decay schedule, following the methodology used in MAE.

3.6 Comparison methods

We began our analysis by comparing MaCo with various pre-training approaches that utilize text as supervision to learn image representations. These approaches include ConVIRT [28], GLoRIA [16], BioViL [17], REFERS [8], MGCA [31], M-FLAG [], Med-UniC [37], M3AE [38], Med-KLIP [5], and MRM [13]. Specifically, ConVIRT proposes to learn medical visual representations by contrasting paired radiographs and sentences from radiology reports. GLoRIA improves upon ConVIRT by contrasting radiograph patches and words in the reports. BioViL and REFERS incorporate masked language modeling loss into contrastive learning, with REFERS introducing a multi-view fusion attention mechanism to better

align the representations of each radiograph and its associated report. M3AE employs mask modeling in both the image and language modalities to investigate the performance of pre-trained models on natural datasets. MedKlip utilizes a report filter to extract medical entities and employs a more complex modal fusion module to aggregate features. MRM leverages a masking mechanism similar to M3AE. Among these different methods, MRM has achieved the most advanced results in the medical field.

To comprehensively evaluate our method, we also introduce some image-based self-supervised learning methods, which include Context Restoration [21], Model Genesis [19], TransVW [22], C2L [20], and ImageNet pre-training [23].

For the phase-grounding tests, we compared our method with two highly relevant approaches, GLoRIA and BioViL. It should be noted that Medclip is not capable of handling free-form text, while MRM and M3AE are unable to achieve zero-shot results due to their training strategy. Finally, we demonstrated the weight visualization of our proposed masked contrastive interaction mechanism, which uses attention maps to indicate that our approach weights the masked image representations in an interpretable manner.

4 Conclusion

Fine-grained knowledge understanding and fine-tuning with limited annotations for downstream tasks pose significant challenges in the development of medical foundation models. In this paper, we propose MaCo, a novel approach that addresses these challenges by achieving granular alignment between radiography and reports and extracting fine-grained representations.

Comprehensive evaluation of the effectiveness of MaCo was conducted utilizing six open-source datasets, involving label-efficient classification and segmentation tasks. The results demonstrated that our proposed MaCo outperformed eight state-of-the-art methods, yielding compelling results. Additionally, we validated the zero-shot ability of MaCo through the phase-grounding task. Both qualitative and quantitative indicators showcased the superiority of MaCo compared to other methods. Furthermore, we quantified the degree of correlation between the location of each radiograph patch and its corresponding report. This analysis highlighted the model’s capability to effectively discriminate regions of reports that the model tends to focus on, enhancing the reliability and acceptability of the model in clinical applications.

During our experiments, we observed some interesting phenomena. We found that methods pre-trained on MIMIC-CXR, which utilize paired radiography and reports, tend to achieve better performance in downstream tasks. We hypothesize that these methods may prioritize the extraction of complementary features from the image and text modalities, leading to improved performance. However, it is important to note that these methods sacrifice their zero-shot capability and related visualizations, which can limit their applicability in diverse clinical environments and hinder the establishment of trust among medical professionals. Fortunately, the slight performance decrease of MaCo in classification tasks can

potentially be compensated by using larger and more diverse datasets, as MaCo employs contrastive learning, which has been shown to have more advantages in the context of large datasets [15, 18, 28, 39].

In conclusion, this paper introduces MaCo, a novel medical foundation model designed to address the challenges of fine-grained knowledge understanding and limited annotation learning in the medical domain. MaCo incorporates granular alignment, leveraging the advantages of both pretext task learning and contrastive learning. The promising results obtained from fine-tuning and zero-shot generalization experiments underscore the potential of MaCo in advancing medical foundation models. This work opens up avenues for further research and development in the field, bringing us towards more effective and generalizable medical AI solutions.

5 Acknowledgments

This research was partly supported by the National Natural Science Foundation of China (62222118, U22A2040), Shenzhen Science and Technology Program (RCYX20210706092104034, JCYJ20220531100213029), Guangdong Provincial Key Laboratory of Artificial Intelligence in Medical Image Analysis and Application (2022B1212010011), the major key project of Peng Cheng Laboratory under grant PCL2023AS1-2, and Key Laboratory for Magnetic Resonance and Multimodality Imaging of Guangdong Province (2020B1212060051).

References

1. Pranav Rajpurkar and Matthew P Lungren. The current and future state of ai interpretation of medical images. *New England Journal of Medicine*, 388(21):1981–1990, 2023.
2. Qi Chang, Zhennan Yan, Mu Zhou, Hui Qu, Xiaoxiao He, Han Zhang, Lohendran Baskaran, Subhi Al’Aref, Hongsheng Li, Shaoting Zhang, et al. Mining multi-center heterogeneous medical data with distributed synthetic learning. *Nature Communications*, 14(1):5510, 2023.
3. Julián N Acosta, Guido J Falcone, Pranav Rajpurkar, and Eric J Topol. Multi-modal biomedical ai. *Nature Medicine*, 28(9):1773–1784, 2022.
4. Michael Moor, Oishi Banerjee, Zahra Shakeri Hossein Abad, Harlan M Krumholz, Jure Leskovec, Eric J Topol, and Pranav Rajpurkar. Foundation models for generalist medical artificial intelligence. *Nature*, 616(7956):259–265, 2023.
5. Chaoyi Wu, Xiaoman Zhang, Ya Zhang, Yanfeng Wang, and Weidi Xie. Medklip: Medical knowledge enhanced language-image pre-training. *medRxiv*, pages 2023–01, 2023.
6. Ekin Tiu, Ellie Talius, Pujan Patel, Curtis P Langlotz, Andrew Y Ng, and Pranav Rajpurkar. Expert-level detection of pathologies from unannotated chest x-ray images via self-supervised learning. *Nature Biomedical Engineering*, 6(12):1399–1406, 2022.
7. Yukun Zhou, Mark A Chia, Siegfried K Wagner, Murat S Ayhan, Dominic J Williamson, Robbert R Struyven, Timing Liu, Moucheng Xu, Mateo G Lozano, Peter Woodward-Court, et al. A foundation model for generalizable disease detection from retinal images. *Nature*, pages 1–8, 2023.
8. Hong-Yu Zhou, Xiaoyu Chen, Yinghao Zhang, Ruibang Luo, Liansheng Wang, and Yizhou Yu. Generalized radiograph representation learning via cross-supervision between images and free-text radiology reports. *Nature Machine Intelligence*, 4(1):32–40, 2022.
9. Kaiming He, Xinlei Chen, Saining Xie, Yanghao Li, Piotr Dollár, and Ross Girshick. Masked autoencoders are scalable vision learners. In *2022 IEEE/CVF Conference on Computer Vision and Pattern Recognition (CVPR)*, pages 15979–15988, 2022.
10. Xiaoman Zhang, Chaoyi Wu, Ya Zhang, Weidi Xie, and Yanfeng Wang. Knowledge-enhanced visual-language pre-training on chest radiology images. *Nature Communications*, 14(1):4542, 2023.
11. Hong-Yu Zhou, Yizhou Yu, Chengdi Wang, Shu Zhang, Yuanxu Gao, Jia Pan, Jun Shao, Guangming Lu, Kang Zhang, and Weimin Li. A transformer-based representation-learning model with unified processing of multimodal input for clinical diagnostics. *Nature Biomedical Engineering*, pages 1–13, 2023.
12. Zhi Huang, Federico Bianchi, Mert Yuksekogunul, Thomas J Montine, and James Zou. A visual–language foundation model for pathology image analysis using medical twitter. *Nature Medicine*, pages 1–10, 2023.
13. Hong-Yu Zhou, Chenyu Lian, Liansheng Wang, and Yizhou Yu. Advancing radiograph representation learning with masked record modeling. *arXiv preprint arXiv:2301.13155*, 2023.
14. Zhihong Chen, Yuhao Du, Jinpeng Hu, Yang Liu, Guanbin Li, Xiang Wan, and Tsung-Hui Chang. Multi-modal masked autoencoders for medical vision-and-language pre-training. In *International Conference on Medical Image Computing and Computer-Assisted Intervention*, pages 679–689. Springer, 2022.

15. Alec Radford, Jong Wook Kim, Chris Hallacy, Aditya Ramesh, Gabriel Goh, Sandhini Agarwal, Girish Sastry, Amanda Askell, Pamela Mishkin, Jack Clark, et al. Learning transferable visual models from natural language supervision. In *International conference on machine learning*, pages 8748–8763. PMLR, 2021.
16. Shih-Cheng Huang, Liyue Shen, Matthew P. Lungren, and Serena Yeung. Gloria: A multimodal global-local representation learning framework for label-efficient medical image recognition. In *2021 IEEE/CVF International Conference on Computer Vision (ICCV)*, pages 3922–3931, 2021.
17. Benedikt Boecking, Naoto Usuyama, Shruthi Bannur, Daniel C Castro, Anton Schwaighofer, Stephanie Hyland, Maria Wetscherek, Tristan Naumann, Aditya Nori, Javier Alvarez-Valle, et al. Making the most of text semantics to improve biomedical vision–language processing. In *European conference on computer vision*, pages 1–21. Springer, 2022.
18. Andrew Ng and Michael Jordan. On discriminative vs. generative classifiers: A comparison of logistic regression and naive bayes. *Advances in neural information processing systems*, 14, 2001.
19. Zongwei Zhou, Vatsal Sodha, Jiaxuan Pang, Michael B Gotway, and Jianming Liang. Models genesis. *Medical image analysis*, 67:101840, 2021.
20. Hong-Yu Zhou, Shuang Yu, Cheng Bian, Yifan Hu, Kai Ma, and Yefeng Zheng. Comparing to learn: Surpassing imagenet pretraining on radiographs by comparing image representations. In *Medical Image Computing and Computer Assisted Intervention–MICCAI 2020: 23rd International Conference, Lima, Peru, October 4–8, 2020, Proceedings, Part I 23*, pages 398–407. Springer, 2020.
21. Liang Chen, Paul Bentley, Kensaku Mori, Kazunari Misawa, Michitaka Fujiwara, and Daniel Rueckert. Self-supervised learning for medical image analysis using image context restoration. *Medical image analysis*, 58:101539, 2019.
22. Fatemeh Haghighi, Mohammad Reza Hosseinzadeh Taher, Zongwei Zhou, Michael B Gotway, and Jianming Liang. Transferable visual words: Exploiting the semantics of anatomical patterns for self-supervised learning. *IEEE transactions on medical imaging*, 40(10):2857–2868, 2021.
23. Xiaosong Wang, Yifan Peng, Le Lu, Zhiyong Lu, Mohammadhadi Bagheri, and Ronald M Summers. Chestx-ray8: Hospital-scale chest x-ray database and benchmarks on weakly-supervised classification and localization of common thorax diseases. In *Proceedings of the IEEE conference on computer vision and pattern recognition*, pages 2097–2106, 2017.
24. Ishan Misra and Laurens van der Maaten. Self-supervised learning of pretext-invariant representations. In *Proceedings of the IEEE/CVF conference on computer vision and pattern recognition*, pages 6707–6717, 2020.
25. Saleh Albelwi. Survey on self-supervised learning: auxiliary pretext tasks and contrastive learning methods in imaging. *Entropy*, 24(4):551, 2022.
26. Ashish Jaiswal, Ashwin Ramesh Babu, Mohammad Zaki Zadeh, Debapriya Banerjee, and Fillia Makedon. A survey on contrastive self-supervised learning. *Technologies*, 9(1):2, 2020.
27. Yuan Jin, Wray Buntine, Francois Petitjean, and Geoffrey I Webb. Discriminative, generative and self-supervised approaches for target-agnostic learning. *arXiv preprint arXiv:2011.06428*, 2020.
28. Yuhao Zhang, Hang Jiang, Yasuhide Miura, Christopher D Manning, and Curtis P Langlotz. Contrastive learning of medical visual representations from paired images and text. In *Machine Learning for Healthcare Conference*, pages 2–25. PMLR, 2022.

29. Zifeng Wang, Zhenbang Wu, Dinesh Agarwal, and Jimeng Sun. Medclip: Contrastive learning from unpaired medical images and text. In *Proceedings of the 2022 Conference on Empirical Methods in Natural Language Processing*, pages 3876–3887, 2022.
30. Shruthi Bannur, Stephanie Hyland, Qianchu Liu, Fernando Perez-Garcia, Maximilian Ilse, Daniel C Castro, Benedikt Boecking, Harshita Sharma, Kenza Bouzid, Anja Thieme, et al. Learning to exploit temporal structure for biomedical vision-language processing. In *Proceedings of the IEEE/CVF Conference on Computer Vision and Pattern Recognition*, pages 15016–15027, 2023.
31. Fuying Wang, Yuyin Zhou, Shujun Wang, Varut Vardhanabhuti, and Lequan Yu. Multi-granularity cross-modal alignment for generalized medical visual representation learning. *Advances in Neural Information Processing Systems*, 35:33536–33549, 2022.
32. Jacob Devlin, Ming-Wei Chang, Kenton Lee, and Kristina Toutanova. Bert: Pre-training of deep bidirectional transformers for language understanding. *arXiv preprint arXiv:1810.04805*, 2018.
33. Alistair EW Johnson, Tom J Pollard, Nathaniel R Greenbaum, Matthew P Lungren, Chih-ying Deng, Yifan Peng, Zhiyong Lu, Roger G Mark, Seth J Berkowitz, and Steven Horng. Mimic-cxr-jpg, a large publicly available database of labeled chest radiographs. *arXiv preprint arXiv:1901.07042*, 2019.
34. Jeremy Irvin, Pranav Rajpurkar, Michael Ko, Yifan Yu, Silvana Ciurea-Ilcus, Chris Chute, Henrik Marklund, Behzad Haghgoo, Robyn Ball, Katie Shpanskaya, et al. Chexpert: A large chest radiograph dataset with uncertainty labels and expert comparison. In *Proceedings of the AAAI conference on artificial intelligence*, volume 33, pages 590–597, 2019.
35. George Shih, Carol C Wu, Safwan S Halabi, Marc D Kohli, Luciano M Prevedello, Tessa S Cook, Arjun Sharma, Judith K Amorosa, Veronica Arteaga, Maya Galperin-Aizenberg, et al. Augmenting the national institutes of health chest radiograph dataset with expert annotations of possible pneumonia. *Radiology: Artificial Intelligence*, 1(1):e180041, 2019.
36. American College of Radiology, American Association of Physicists in Medicine (AAPM), et al. Society for imaging informatics in medicine (siim). *Practice guideline for digital radiography (Resolution 42, adopted in 2007)[visionato il 4 dicembre 2012]. Disponibile su: www.siiimweb.org*, 2014.
37. Zhongwei Wan, Che Liu, Mi Zhang, Jie Fu, Benyou Wang, Sibao Cheng, Lei Ma, César Quilodrán-Casas, and Rossella Arcucci. Med-unic: Unifying cross-lingual medical vision-language pre-training by diminishing bias. *arXiv preprint arXiv:2305.19894*, 2023.
38. Xinyang Geng, Hao Liu, Lisa Lee, Dale Schuurmans, Sergey Levine, and Pieter Abbeel. Multimodal masked autoencoders learn transferable representations. *arXiv preprint arXiv:2205.14204*, 2022.
39. Rajat Raina, Yirong Shen, Andrew McCallum, and Andrew Ng. Classification with hybrid generative/discriminative models. *Advances in neural information processing systems*, 16, 2003.